



HAL
open science

Post-Combustion CO₂ Capture by Vacuum Swing Adsorption Using Zeolites – a Feasibility Study

G. D. Pirngruber, V. Carlier, D. Leinekugel-Le-Cocq

► **To cite this version:**

G. D. Pirngruber, V. Carlier, D. Leinekugel-Le-Cocq. Post-Combustion CO₂ Capture by Vacuum Swing Adsorption Using Zeolites – a Feasibility Study. Oil & Gas Science and Technology - Revue d'IFP Energies nouvelles, 2014, 69 (6), pp.989-1003. 10.2516/ogst/2012067 . hal-01933518

HAL Id: hal-01933518

<https://ifp.hal.science/hal-01933518>

Submitted on 23 Nov 2018

HAL is a multi-disciplinary open access archive for the deposit and dissemination of scientific research documents, whether they are published or not. The documents may come from teaching and research institutions in France or abroad, or from public or private research centers.

L'archive ouverte pluridisciplinaire **HAL**, est destinée au dépôt et à la diffusion de documents scientifiques de niveau recherche, publiés ou non, émanant des établissements d'enseignement et de recherche français ou étrangers, des laboratoires publics ou privés.



This paper is a part of the hereunder thematic dossier published in OGST Journal, Vol. 69, No. 6, pp. 977-1129 and available online [here](#)

Cet article fait partie du dossier thématique ci-dessous publié dans la revue OGST, Vol. 69, n°6, pp. 977-1129 et téléchargeable [ici](#)

DOSSIER Edited by/Sous la direction de : **P.-L. Carrette**

PART 2

Post Combustion CO₂ Capture Captage de CO₂ en postcombustion

Oil & Gas Science and Technology – Rev. IFP Energies nouvelles, Vol. 69 (2014), No. 6, pp. 977-1129

Copyright © 2014, IFP Energies nouvelles

- 977 > Editorial
- 989 > *Post-Combustion CO₂ Capture by Vacuum Swing Adsorption Using Zeolites – a Feasibility Study*
Captage du CO₂ en postcombustion par adsorption modulée en pression avec désorption sous vide sur zéolithes — étude de faisabilité
G. D. Pirngruber, V. Carlier and D. Leinekugel-le-Cocq
- 1005 > *Membrane Separation Processes for Post-Combustion Carbon Dioxide Capture: State of the Art and Critical Overview*
Procédés membranaires pour le captage du dioxyde de carbone : état de l'art et revue critique
B. Belaisaoui and É. Favre
- 1021 > *Pressure Drop, Capacity and Mass Transfer Area Requirements for Post-Combustion Carbon Capture by Solvents*
Pertes de charge, capacité et aires de transfert de matière requises pour le captage du CO₂ en postcombustion par solvants
A. Lassauce, P. Alix, L. Raynal, A. Royon-Lebeaud and Y. Haroun
- 1035 > *Hollow Fiber Membrane Contactors for Post-Combustion CO₂ Capture: A Scale-Up Study from Laboratory to Pilot Plant*
Captage postcombustion du CO₂ par des contacteurs membranaires de fibres creuses : de l'échelle laboratoire à l'échelle pilote industriel
É. Chabanon, E. Kimball, É. Favre, O. Lorain, E. Goetheer, D. Ferre, A. Gomez and P. Broutin
- 1047 > *Hollow Fiber Membrane Contactors for CO₂ Capture: Modeling and Up-Scaling to CO₂ Capture for an 800 MW_e Coal Power Station*
Contacteurs à membrane à fibres creuses pour la capture de CO₂ : modélisation et mise à l'échelle de la capture du CO₂ d'une centrale électrique au charbon de 800 MW_e
E. Kimball, A. Al-Azki, A. Gomez, E. Goetheer, N. Booth, D. Adams and D. Ferre
- 1059 > *Regeneration of Alkanolamine Solutions in Membrane Contactor Based on Novel Polynorbornene*
Régénération de solutions d'alcanolamine dans un contacteur à membrane basé sur un nouveau polynorbornène
A.A. Shutova, A.N. Trusov, M.V. Bermeshev, S.A. Legkov, M.L. Gringolts, E.Sh. Finkelstein, G.N. Bondarenko and A.V. Volkov
- 1069 > *Development of HiCapt+™ Process for CO₂ Capture from Lab to Industrial Pilot Plant*
Développement du procédé HiCapt+™ pour le captage du CO₂ : du laboratoire au pilote industriel
É. Lemaire, P. A. Bouillon and K. Lettat
- 1081 > *A Technical and Economical Evaluation of CO₂ Capture from Fluidized Catalytic Cracking (FCC) Flue Gas*
Évaluation technico-économique du captage du CO₂ présent dans les fumées d'une unité FCC (Fluidized Catalytic Cracking)
R. Digne, F. Feugnet and A. Gomez
- 1091 > *Pilot Plant Studies for CO₂ Capture from Waste Incinerator Flue Gas Using MEA Based Solvent*
Étude du captage du CO₂ dans des gaz de combustion d'un incinérateur de déchets à l'aide d'un pilote utilisant un solvant à base de MEA
I. Aouini, A. Ledoux, L. Estel and S. Mary
- 1105 > *Amine Solvent Regeneration for CO₂ Capture Using Geothermal Energy with Advanced Stripper Configurations*
Régénération d'un solvant de captage du CO₂ utilisant l'énergie géothermique et des configurations améliorées pour le régénérateur
D.H. Van Wagener, A. Gupta, G.T. Rochelle and S.L. Bryant
- 1121 > *ACACIA Project – Development of a Post-Combustion CO₂ capture process. Case of the DMX™ process*
Projet ACACIA – Développement d'un procédé de captage du CO₂ postcombustion – Cas du procédé DMX™
A. Gomez, P. Briot, L. Raynal, P. Broutin, M. Gimenez, M. Soazic, P. Cessat and S. Saisset

Post-Combustion CO₂ Capture by Vacuum Swing Adsorption Using Zeolites – a Feasibility Study

G. D. Pirngruber*, V. Carlier and D. Leinekugel-le-Cocq

IFP Energies nouvelles, Rond-point de l'échangeur de Solaize, BP 3, 69360 Solaize - France
e-mail: gerhard.pirngruber@ifpen.fr - vincent.carlier27@gmail.com - damien.leinekugel@ifpen.fr

* Corresponding author

Résumé — Captage du CO₂ en postcombustion par adsorption modulée en pression avec désorption sous vide sur zéolithes — étude de faisabilité — Les résultats de simulation issus de la littérature suggèrent que les procédés d'adsorption modulée en pression avec désorption sous vide (*Vacuum Swing Adsorption*, VSA) employant un physisorbant sont nettement moins efficaces d'un point de vue énergétique que le procédé de référence de captage de CO₂ par absorption aux amines. La plupart des études considèrent la zéolithe NaX comme adsorbant. La NaX présente une très forte affinité pour le CO₂, mais elle est difficile à régénérer et est très sensible à la présence d'eau dans les fumées. Jouer sur la polarité de l'adsorbant doit permettre de trouver un meilleur compromis entre capacité d'adsorption, caractère régénérable et sensibilité à l'eau. C'est pourquoi, dans cette contribution, nous avons testé une série de zéolithes afin d'évaluer leur performances comme physisorbants dans un procédé de captage de CO₂ par VSA. Les adsorbants sont testés par adsorption de fumées modèles sèches et humides sur un lit d'adsorbant, en perçage et en conditions cycliques. Le matériau le plus intéressant, la zéolithe EMC-1, est choisi pour la simulation d'un cycle VSA complet, en comparaison avec la NaX. Les deux adsorbants atteignent les objectifs en termes de rendement (>90 %) et de pureté du CO₂ (>95 %), mais le très faible niveau de pression nécessaire à la régénération de l'adsorbant sera un handicap de poids pour l'utilisation de cette technologie à grande échelle.

Abstract — Post-Combustion CO₂ Capture by Vacuum Swing Adsorption using Zeolites — a Feasibility Study — Simulation results in the literature suggest that Vacuum Swing Adsorption (VSA) processes using physisorbents might largely outperform the current state-of-the-art post-combustion CO₂ capture technologies based on amine solvents in terms of energy consumption. Most studies consider the zeolite NaX as adsorbent. NaX has a very strong affinity for CO₂ but is difficult to regenerate and very sensitive to the presence of water in the flue gas. By tuning the polarity of the adsorbent, it might be possible to find a better compromise between adsorption capacity, regenerability and sensitivity to H₂O. In the present contribution, we therefore screen the performance of a series of zeolites as physisorbents in a VSA process for CO₂ capture. The adsorbents are tested by breakthrough experiments of a dry and wet model flue gas, in once-through and cyclic operation. The most interesting material, zeolite EMC-1, is selected for numerical simulations of a full VSA cycle, in comparison with zeolite NaX. Both solids satisfy the performance targets in terms of recovery (>90%) and purity of CO₂ (>95%) but the very low pressure required for regeneration of the adsorbents will be a serious handicap for the deployment of this technology on a large scale.

INTRODUCTION

There is now general consensus that the concentration of CO₂ in the atmosphere needs to be stabilized at a level of 450 ppm in order to limit the extent of global warming. In order to achieve this target, a series of measures will be necessary: increasing energy efficiency, shifting to energy sources that produce little or no CO₂ emissions (wind, solar, nuclear, biomass, etc.) and, last but not least, employing CCS technology (Carbon Capture and Storage) to large CO₂ emitters, in particular to coal firing power plants. Scenarios show that a ~ 20% contribution of CCS is needed in order to stabilize the CO₂ concentration at the desired level. There are different ways to deploy CCS: one distinguishes oxy-combustion, pre-combustion CO₂ capture and post-combustion CO₂ capture. We are here concerned with post-combustion CO₂ capture, which is the technology that can be most easily applied in existing coal/petroleum firing power plants, refineries, etc., by “simply” adding a CO₂ capture unit to the plant. Post-combustion CO₂ capture acts on the flue gases produced by combustion. CO₂ in these flue gases is diluted (10-15%) and at low pressure (total pressure is ~ 1 bar), which makes CO₂ removal difficult.

The current state-of-the-art post-combustion capture technology is absorption of CO₂ by an aqueous Mono-EthanolAmine (MEA) solution. MEA has a very strong affinity to CO₂ and captures CO₂ efficiently even at low partial pressure but the regeneration of the solvent by heating requires a large amount of energy [1, 2]. Moreover, degradation of the amine by oxygen in the flue gas causes corrosion problems and leads to a high net consumption of solvent (> 1.4 kg MEA/t CO₂ captured, *i.e.* > 4 700 t per year for a 600 MW power plant). Therefore an intensive search for alternative solutions is going on. One of the options is to use Pressure (or Vacuum) Swing Adsorption (PSA or VSA) technology in combination with solid sorbents. PSA/VSA technology is proven and robust, it avoids the difficulties associated with the handling of liquids. The challenge is, however, to find appropriate sorbents. Post-combustion flue gases typically contain 10-15% CO₂, 8-15% H₂O, 3-4% O₂, traces of NO_x and SO_x (depending on the DeNO_x and DeSO_x treatment), the balance being N₂. The objective is to capture a high fraction of the CO₂ (90%) and to recover the CO₂ at high purity. The fraction of non-condensable impurities (*i.e.* N₂, O₂) must be below 4% in order to allow the compression of CO₂ for its transport to the storage site. We therefore need highly selective CO₂ sorbents. That is why many amine-based solid sorbents have been studied for post-combustion CO₂ capture [3-9]. Amines can be immobilized on a solid support either by impregnation or by grafting [10]. The acid-base interaction between amino groups and CO₂ assures a very high selectivity towards sorption of CO₂. The presence of water in the flue gas does not interfere with this acid-base interaction. In some cases, the CO₂ capacity is even

enhanced in the presence of water because the formation of bicarbonates becomes possible [11, 12]. Immobilized amines mimic the chemistry of amine based solvents, hence, we find their strengths but also their weaknesses. The strong chemisorption leads to a high CO₂ adsorption capacity at low pressure, the CO₂/N₂ selectivity is quasi infinite but regeneration is rather difficult and degradation may occur. There are also health and safety concerns about the contamination of the decarbonized flue gas by volatilization of the amine or its degradation products.

Another option is the use of physisorbents, like zeolites or Metal Organic Frameworks (MOF). It is well known that polar zeolites like NaX or zeolite 5A are very good adsorbents for CO₂, even at low partial pressures. The adsorption capacity at 0.15 bar is about 3 mol/kg [13], which is comparable to the best amine-based solid sorbents. The CO₂/N₂ selectivity of NaX is also extremely high, above 100 [14]. Similar results are obtained for zeolite 5A [15]. The high capacity and selectivity are a result of the high polarity of the zeolites NaX and 5A. The quadrupole moment of CO₂ strongly interacts with the electric field generated by the extra-framework cations of the zeolite. Metal organic frameworks belonging to the CPO-27 structure type have even higher adsorption capacities than zeolites NaX or 5A under the conditions relevant for CO₂ capture, *i.e.* at a partial pressure of CO₂ of about 0.1 bar [16]. The CPO-27 structure is characterized by the presence of coordinatively unsaturated metal centers, which have a strong affinity for CO₂, similar to the role of the extra-framework cations in zeolites.

A fundamental problem in the design of physisorbents for CO₂ capture is that these materials systematically prefer the adsorption of H₂O over the adsorption of CO₂. Flue gases fatally contain humidity (at low temperatures they are even saturated with humidity). The CO₂ adsorption capacity of NaX, for example, decreases by 99% in humid streams [17], because water is preferentially adsorbed over CO₂. The MOF structures CPO-27-Ni and HKUST-1 are somewhat less sensitive to water than zeolites NaX and 5A but the inhibition of CO₂ adsorption remains very important [16]. Only purely siliceous, defect-free zeolites have been reported to be entirely hydrophobic [18] but these solids are entirely devoid of polarity and therefore have a very low adsorption capacity for CO₂ [19], as well. The dilemma is that a certain polarity of the adsorbent is needed to assure a high adsorption capacity of CO₂ and a high CO₂/N₂ selectivity. Since polarity and hydrophilicity are intimately linked with each other, a high polarity necessarily implies that H₂O will be adsorbed even more strongly and hence strongly inhibit the adsorption of CO₂.

The challenge, therefore, is to tune the polarity of the adsorbent to an intermediate level, so as to find the best compromise between CO₂ adsorption capacity, CO₂/N₂ selectivity, easy of regeneration under vacuum and inhibition by H₂O. Palomino *et al.* [20] nicely demonstrated that the CO₂

adsorption and separation properties can be finely tuned by varying the Si/Al ratio, *i.e.* the polarity, of the framework. In the present study, we have therefore studied the performance of a series of zeolites with varying Si/Al ratios. The adsorption capacity and regenerability of the materials was evaluated by breakthrough experiments with a CO₂/N₂ feed mixture. Also, the water tolerance of the materials was tested. The most promising material was then selected for numerical simulations of a full VSA cycle, in comparison with zeolite NaX.

1 EXPERIMENTAL SECTION

1.1 Adsorbents

The adsorption measurements were carried out on commercial zeolites purchased from Zeolyst (*Tab. 1*): two mordenites with different Si/Al ratios and two USY zeolites with different Si/Al ratios. Of these four samples, only the CVB10a was in the Na⁺ form, the other zeolites have NH₄⁺ as extra-framework cation. The NH₄⁺ zeolites were transformed into Na⁺ zeolites by a three-fold ion exchange with a 0.5 molar solution of NaCl at 363 K. A reference sample of zeolite NaX was provided by CECA.

In addition to the commercial zeolites, a synthetic EMC-1 (FAU-type zeolite) with a Si/Al ratio of 3.9 was tested. This zeolite was prepared according to the recipe described by Chatelain *et al.* [21]. A starting gel having the following molar composition: 10 SiO₂ : 1 Al₂O₃ : 2.1 Na₂O : 0.5 (15-Crown-5) : 100 H₂O was prepared by mixing 55.5 g of 40 wt% silica sol (Ludox HS40, *Dupont*), 6.9 g of sodium aluminate (56% Al₂O₃, 37% Na₂O, *Carlo Erba*), 4.1 g of crown ether (15-crown-5, 98%, *Aldrich*), 2.56 g of sodium hydroxyde (98%, *Fluka*) and 30.9 g of water (desionized water, 18 MΩ). This zeolite was synthesised hydrothermally

TABLE 1

Global and framework Si/Al ratio, Na-content, surface area and micropore volume of the samples

Sample	Si/Al	Si/Al _f	Wt% Na	S _{BET} (m ² /g)	V _{micro} (cm ³ /g)
Na-MOR-6 (CBV10a)	6.2	8	4.8%	415	
NH ₄ -MOR-10 (CBV21a) ^a	10		0.06%	424	0.17
Na-MOR-10			2.78%		
NH ₄ -USY-6 (CBV712) ^a	6	11	0.04%	791	0.27
Na-USY-6			1.3%		
NH ₄ -USY-15 (CBV720) ^a	15.2	25	0.02%	805	0.25
Na-USY-15			1.07%		
EMC-1	3.9		6.02%	780	0.33
NaX	1.3	1.3	9.68%	816	0.34

^a NH₄-zeolites are transformed into H-zeolites by thermal activation before testing.

in a 100 mL stainless steel autoclave at 110°C for 8 hours. After cooling to room temperature, the crystals were filtered on a Buchner funnel, and washed thoroughly with deionized water. The products were dried overnight at 100°C and calcined at 550°C under air during 8 hours.

The Si/Al ratio of the zeolites was determined by X-ray fluorescence. The USY zeolites contain quite a high fraction of extra-framework Al. The actual framework Si/Al ratio was therefore estimated from ²⁹Si-NMR and IR spectroscopy. The Na-content of the materials was determined from atomic absorption spectroscopy.

The porosity of the adsorbents was characterized by their N₂ adsorption isotherm at 77 K (measured on a Micromeritics ASAP 2010). BET surface areas and micropore volumes (obtained from a t-plot) are compiled in Table 1.

1.2 Breakthrough Experiments

The adsorbents were filled into a column that was placed into an oven. A gas distribution system allowed us to feed the column either with pure N₂ or with a mixture of CO₂ in N₂ and to switch rapidly between the two. Moreover, we had the possibility to introduce water vapour into the feed stream by passing *via* a saturator. The pressure was always atmospheric plus the (small) pressure drop over the column (between 0.1 and 1 bar, depending on the adsorbent). The sorbents were initially treated in N₂ at 623 K for 2 h and then brought to the adsorption temperature (323 K) and a breakthrough curve N₂ → N₂ + CO₂ was recorded by means of a TCD detector at the column exit. Adsorption isotherms of CO₂ were measured by repeating the breakthrough experiments at different CO₂ concentrations (from 5 to 30%), each time followed by a regeneration at 623 K for 2 h. Note that these isotherms are in fact CO₂/N₂ co-adsorption isotherms but the amount of adsorbed N₂ was not quantified. In addition to the adsorption isotherms, cyclic adsorption-desorption experiments were performed. In that case, the CO₂ concentration was fixed at 15% and the feed was alternated between CO₂ + N₂ and N₂, while keeping the temperature constant. These cyclic adsorption experiments give us information on the regenerability of the samples.

For evaluating the influence of humidity on adsorption, the following procedure was used. The N₂ stream was passed through a saturator that was filled with distilled water and thermostated at 306 K (which corresponds to a vapour pressure of 5 kPa) for 1 h before starting the breakthrough experiment. During the whole breakthrough experiment the partial pressure of H₂O was maintained at 5 kPa by passing through the saturator. At the column exit water was condensed in a cool bath (at 273 K) so as to enter with a gas of constant humidity into the TCD detector. After breakthrough the feed was switched back to humid N₂ and the breakthrough experiment with humid feed was repeated at intervals of several hours.

Breakthrough experiments for measuring the CO₂/N₂ selectivity were carried out on a different experimental setup. Activation was carried out in a non-adsorbable carrier gas (He) and the breakthrough curve was triggered by switching from He to a 50/50 mixture of CO₂/N₂. The CO₂ and N₂ concentrations at the column exit were measured by a mass spectrometer, following the procedure described in [22]. The experiments were carried out at 303 K. At least four breakthrough/desorption measurements were carried out with each adsorbent:

- a step from He to CO₂/N₂, followed by a step back to He;
- a step from pure CO₂ to CO₂/N₂, followed by a step back to He.

The adsorbed amount of CO₂ was determined from the step He → CO₂/N₂, the amount of N₂ was obtained by averaging the results of the four breakthrough/desorption curves. For an equimolar feed mixture of CO₂/N₂ the adsorption selectivity α simply corresponds to the ratio of the adsorbed amounts of CO₂ and N₂.

2 RESULTS

2.1 Adsorption Isotherms

Figure 1 compares the adsorption isotherms of CO₂ over three different mordenite samples. It clearly shows the influence of Si/Al ratio and of the extra-framework cation on the adsorption properties. The sample with the lower Si/Al ratio has the higher adsorption capacity. Moreover,

Na⁺-exchanged samples adsorb more CO₂ than H-mordenite (activation transforms NH₄-mordenite into H-mordenite). It has already been shown before that Na-ZSM-5 has a higher heat of adsorption than H-ZSM-5 [23]. The electrostatic interaction between the Na⁺ cations and the quadrupole moment of CO₂ is stronger than that of a largely covalent Bronsted OH-group.

The trends observed for mordenite are confirmed with the faujasite adsorbents (Fig. 2). The CO₂ adsorption capacity decreases with increasing Si/Al ratio and NH₄-exchanged samples adsorb much less CO₂ than Na-faujasites. Zeolite NaX has by far the highest adsorption capacity because its Si/Al ratio is much lower than that of the other faujasites. At similar Si/Al ratio, the CO₂ isotherms of the Na-faujasite samples are not as steep as the isotherms of Na-mordenites. The strong initial adsorption of CO₂ in mordenite may be related to the strong confinement in the side pockets of the mordenite structure.

In order to rationalize the adsorption data on the series of faujasite and mordenite samples, the isotherms were fitted by a Langmuir model:

$$q = q_{sat} \cdot \frac{b \cdot p_{CO_2}}{1 + b \cdot p_{CO_2}}$$

The Henry constants of the isotherms were then calculated from $K_{Henry} = b \times q_{sat}$.

Figure 3 shows that the Henry constants are correlated with the Na content of the zeolites, which indicates that the Na⁺ cations are the preferred adsorption sites of CO₂. The Na content can, therefore, be regarded as a good semi-quantitative indicator of the polarity of the zeolite. The slope of the curve

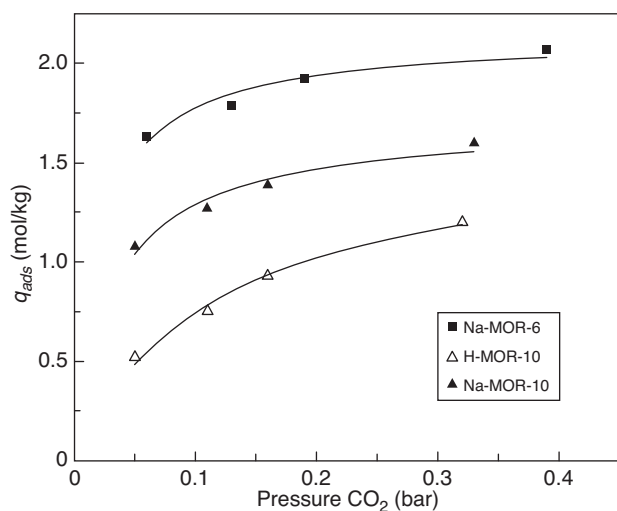


Figure 1

Adsorption isotherms of CO₂ (in mixture with N₂) at 323 K over three different mordenite samples.

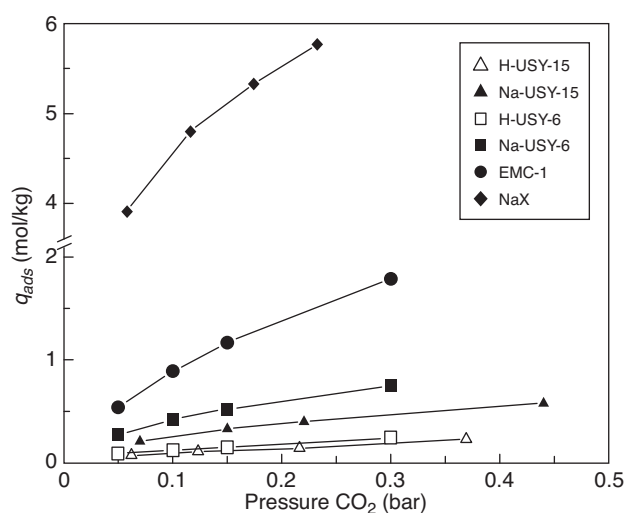


Figure 2

Adsorption isotherms of CO₂ (in mixture with N₂) at 323 K over different faujasite samples.

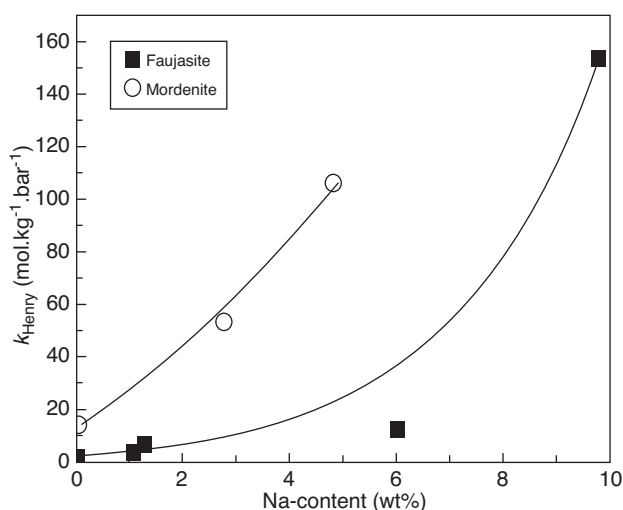


Figure 3

Henry constants of the CO₂ isotherms at 323 K as a function of the Na content of the zeolites.

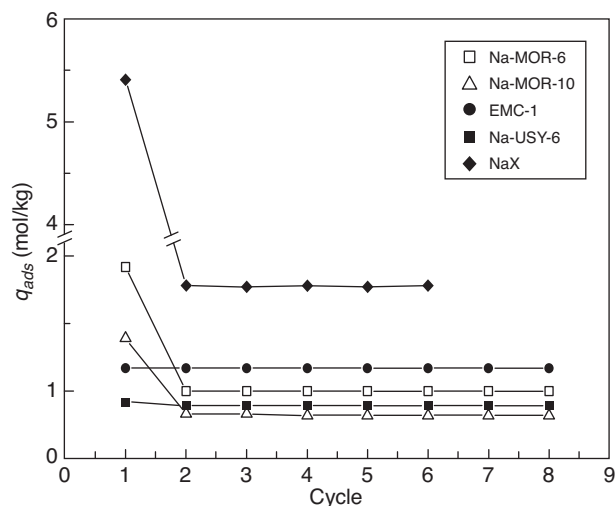


Figure 4

Adsorption capacity over several adsorption-desorption cycles at 323 K. CO₂ concentration 15% in N₂, desorption by N₂ purge for 30 min.

K_{Henry} vs Na-content is much higher on mordenite than on faujasite. In mordenite, the electrostatic effect of the Na⁺ cations is exacerbated by a stronger confinement, *i.e.* a smaller pore size.

2.2 Adsorption — Desorption Cycles

A high adsorption capacity at the working pressure of the process is not a sufficient criterion for the selection of an adsorbent. The adsorbent must also be easily regenerable

upon depressurisation and desorption under vacuum. The quantity that can be adsorbed and desorbed over many adsorption/desorption cycles is called the working capacity of the adsorbent. Since our experimental setup did not allow us to regenerate the adsorbents under vacuum, we established a qualitative ranking of their regenerability, by desorbing CO₂ via a N₂ purge gas for 30 min at 323 K (*i.e.* under isothermal conditions). The results are shown in Figure 4. With the exception of NaX, the faujasite adsorbents were perfectly regenerable by the N₂ purge and the adsorption capacity remained constant during 8 adsorption/desorption cycles. The two Na-mordenites lost a significant fraction of their initial adsorption capacity when going from the 1st to the 2nd cycle, *i.e.* they were not fully regenerable by a N₂ purge. Also in the case of NaX, 30 min were largely insufficient to desorb CO₂ from the column. As expected, the regenerability was related to the shape of the isotherm at low pressure. Very steep isotherms (*i.e.* NaX, Na-MOR-6, Na-MOR-10) mean difficult regeneration. In spite of its bad regenerability, the best cyclic capacity was obtained with NaX (1.8 mol/kg), followed by EMC-1 (1.2 mol/kg).

2.3 CO₂/N₂ Selectivity

The CO₂/N₂ selectivity was measured by breakthrough experiments with 50/50 mixtures of CO₂/N₂.

Figure 5 compares the breakthrough curves of EMC-1, Na-USY-15 and Na-MOR-10. One can immediately see that the quality of the CO₂/N₂ separation was less good on Na-USY-15. The selectivity values are reported in Table 2⁽¹⁾. Both Na-mordenites as well as NaX and EMC-1 had selectivities above 40 (all selectivities above 40 were considered to be equal because of the large experimental error). In the case Na-USY-15, which is the least polar sample that was tested, the selectivity dropped significantly to 11. This suggests that there is a minimum polarity above which there is no measurable gain in the CO₂/N₂ selectivity any more. For faujasite samples, this threshold is somewhere between Na-USY-15 and EMC-1.

TABLE 2

Results of breakthrough experiments of a 50/50 CO₂/N₂ mixture at 303 K

	Q _{ads} CO ₂ (mol/kg)	Q _{ads} N ₂ (mol/kg)	Selectivity
NaX	5.46	0.10 ± 0.04	54 ± 22
EMC-1	2.84	0.06 ± 0.03	44 ± 22
Na-USY-15	1.16	0.11 ± 0.03	11 ± 3
Na-MOR-6	3.23	0.08 ± 0.04	42 ± 25
Na-MOR-10	2.42	0.03 ± 0.01	80 ± 30

¹ The adsorbed amount of N₂ is very small. We, therefore, averaged results from several tests to obtain fairly reliable results.

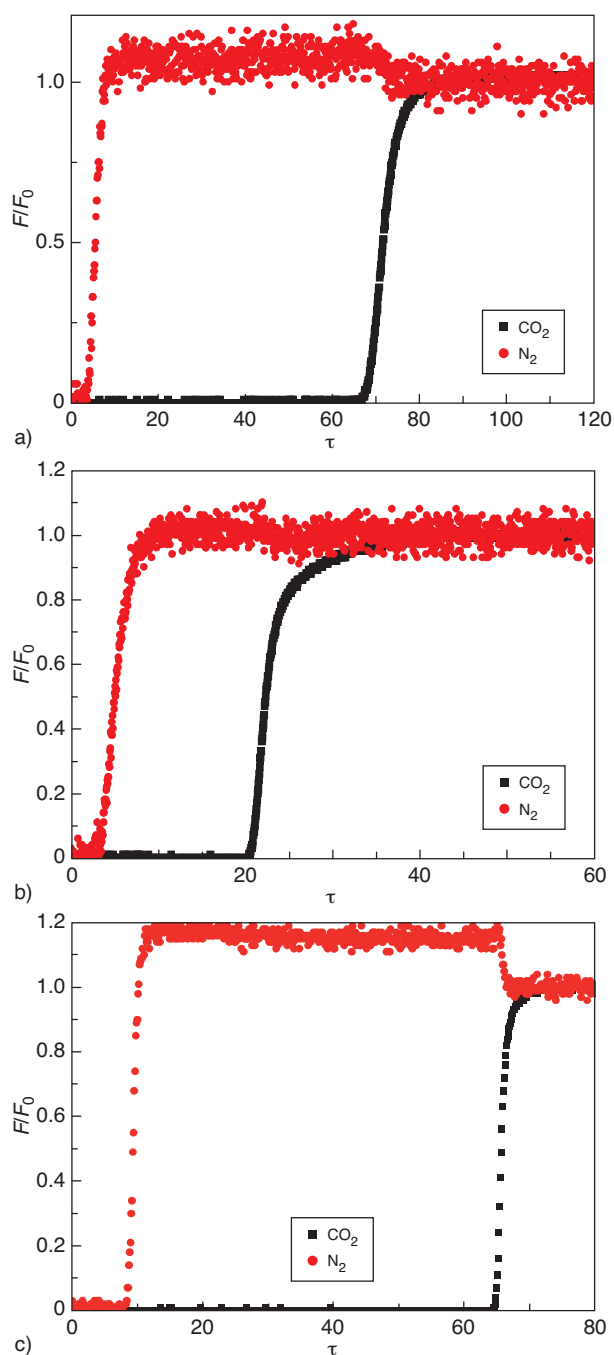


Figure 5

Breakthrough curves of a 50/50 mixture of CO_2/N_2 over a) EMC-1, b) Na-USY-15, c) Na-MOR-10. F/F_0 = normalized molar flow rate at column exit (F_0 = feed flow rate). τ = time/contact time.

2.4 Inhibition by H_2O

As a next step, we evaluated the effect of humidity on CO_2 adsorption. Breakthrough experiments were carried out with humid gases, *i.e.* by switching from a mixture $\text{N}_2 + \text{H}_2\text{O}$ to a

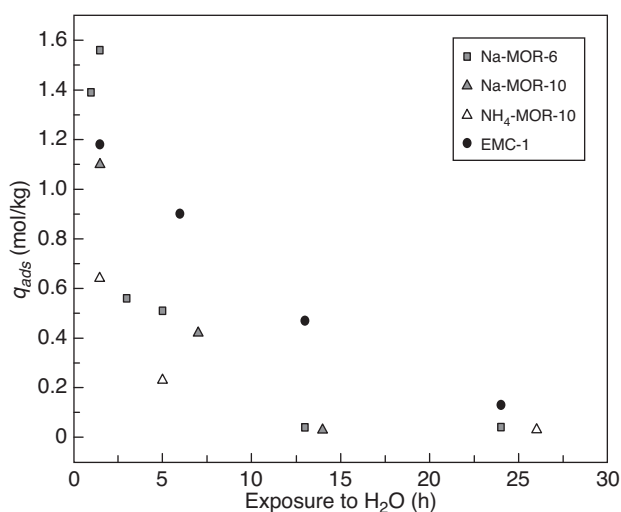


Figure 6

CO_2 adsorption capacity in a humid feed (15% CO_2 , 5% H_2O) as a function of the total exposure time of the adsorbent to a humid gas.

mixture of $\text{N}_2 + \text{CO}_2 + \text{H}_2\text{O}$. The H_2O content was regulated by a saturator, which was thermostated at 306 K. This corresponds to a vapor pressure of 0.05 bar and a relative humidity of 43% at 323 K. The adsorbent was exposed to the $\text{N}_2 + \text{H}_2\text{O}$ mixture for 1 h before adding CO_2 to the feed. For the three mordenite samples, the CO_2 adsorption capacity dropped by 0.3 mol/kg compared to a dry feed. For EMC-1, no significant change was observed. We noticed, however, that the CO_2 capacity dropped more strongly when the initial exposure to the $\text{N}_2 + \text{H}_2\text{O}$ mixture was prolonged (Fig. 6). That made us suspect that the solids were not yet saturated with H_2O . We therefore carried out several successive breakthrough experiments, at increasing total exposure times to H_2O . Figure 6 shows that the CO_2 adsorption capacity rapidly decreases with increasing exposure time to humid feed. Already after 15 h of exposure to 5% H_2O , the adsorption capacity of CO_2 has dropped almost to zero. 10 h corresponds roughly to the time needed to saturate the pore volume of mordenite with water under our conditions (concentration and flow rate). We can deduce that the pore volume of mordenite is indeed gradually filled with H_2O . As soon as the whole column is saturated with H_2O hardly any CO_2 can be adsorbed any more. In the case of EMC-1, the CO_2 adsorption capacity decreases more gradually, which is probably due to the higher pore volume of EMC-1, *i.e.* it takes more time to fill the pores with H_2O but the principle remains the same.

These results confirm that even zeolites with moderate polarity like H-MOR-10 largely prefer the adsorption of H_2O over the adsorption of CO_2 . This does not mean that it is impossible to run a CO_2 adsorption process with zeolites in the presence of H_2O but a large part of the bed will be

monopolized by the adsorption of H₂O and not be effective at all for CO₂ capture. Since water has a very strong affinity for zeolites its regeneration will be very difficult. It makes more sense to remove the bulk of the water content by “weaker” adsorbents, like silica gel, alumina or activated carbons [24].

3 MODELING OF THE VSA CO₂ CAPTURE PROCESS

After having presented the adsorption properties of a series of zeolites, we now turn to the chemical engineering aspects of a CO₂ capture process by VSA. We first discuss the technical boundary conditions, then describe the numerical modeling of the VSA process and finally discuss the industrial feasibility of CO₂ by VSA.

3.1 Boundary Conditions

Any process for CO₂ capture from flue gases must fulfill two technical targets:

- achieve a high CO₂ recovery;
- produce a CO₂ of high purity that is suited for sequestration.

The optimum recovery level is defined by the trade-off between recovery and cost, *i.e.* by minimizing the price of avoided CO₂. The energy consumption (per captured CO₂) of a VSA process increases with increasing recovery (as will be discussed later). On the other hand, the capital expenses for constructing a CO₂ capture plant do not depend much on the recovery and will, therefore, contribute more heavily to the overall cost, when the recovery is low. Many studies consider a recovery level of 90%, so we started out by fixing our target recovery to this value.

The technical constraint in terms of purity of the CO₂ is stricter. The level of non-condensable impurities, *i.e.* N₂ and O₂, must be below 4% in order to facilitate the compression of CO₂ to a supercritical state, for the purpose of transport and sequestration.

Purity strongly depends on the selectivity of the adsorbent. At the end of the adsorption step, some N₂ (and O₂) is co-adsorbed on the zeolite and some is present in the interstitial volume of the bed. In order to achieve 96% purity, a large fraction of the N₂ must be removed from the bed before the CO₂ recovery step. This can be achieved by modifications of the VSA cycle [25-28]. A co-current depressurisation of the bed, at the end of the adsorption step, releases a large fraction of the N₂ from the interstitial volume and allows advancing the concentration front of CO₂ towards to end of the bed, without sacrificing recovery, since the effluent of the depressurisation step is recycled for repressurisation of another bed. Additionally, a CO₂ rinse step, in which part of the recovered CO₂ is recycled to the bed, may be added in order to displace co-adsorbed N₂ from the adsorbent. Depressurisation and CO₂ rinse may be combined. The lower the pressure of the CO₂ rinse step P_R is chosen, the smaller is the amount of CO₂ required for purging the column and the smaller is the energy consumption for compressing the CO₂ recycle stream to P_R . In order to maintain a high recovery of CO₂, the effluent of the depressurization step is usually used to repressurize another column to an intermediate pressure P_I (Fig. 7). In that case, the condition $P_R > P_I$ puts an upper limit on the amount of gas that can be used for repressurization, which indirectly imposes a lower limit on P_R .

After having removed a large fraction of N₂ and O₂ from the column by depressurization and purge, CO₂ is recovered by lowering the pressure, *i.e.* by pulling vacuum. In conventional PSA processes, the column is further regenerated

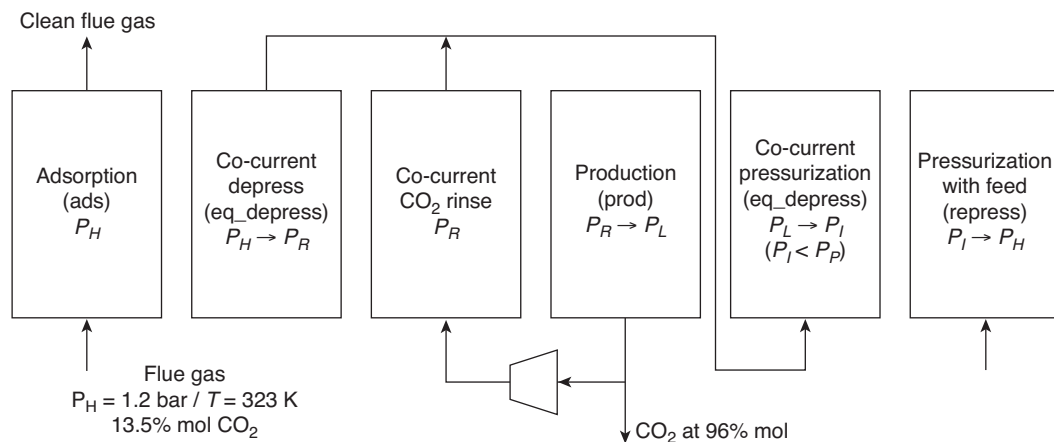


Figure 7

VSA cycle for CO₂ capture from flue gas.

by a purge with the light product, so as to perfectly clean the light product end of the column but, in the present case, it is not possible to employ a purge with a non-condensable gas like N_2 (*vide infra*), because of the stringent purity requirements in CO_2 capture. Therefore, at the end of the CO_2 recovery step, the light product end of the column is in equilibrium with almost pure CO_2 at the partial pressure of regeneration (plus the pressure drop in the column). In the following adsorption step, CO_2 cannot be adsorbed beyond that equilibrium partial pressure, leading to a permanent slip of CO_2 that limits the recovery. For example, if the adsorption is carried out at a pressure of 1.2 bar and the CO_2 concentration is 15%, the pressure of regeneration must be below 0.018 bar in order to be able to achieve a recovery of 90%. An examination of earlier simulation and experimental work on VSA for CO_2 capture confirms that recovery is limited by the ratio between the partial pressures of CO_2 in the feed step and in the regeneration step [29, 30], if the column is not purged with light product.

In order to be able to circumvent the use of such low pressures for regeneration, one would have to find another way to clean the light product end of the bed before starting a new adsorption step. Many VSA simulation studies employ a low pressure purge with light product (N_2) but, as already mentioned above, a N_2 purge necessarily pollutes the CO_2 product and makes it impossible to achieve the 96% purity [27, 28, 31]. An alternative is to repressurize the column from the light product end with N_2 (instead of repressurizing with feed). This method can be effective for adsorbents with a low CO_2/N_2 selectivity, like activated carbons. On an activated carbon N_2 competes with CO_2 for adsorption sites and a repressurization by N_2 can push the concentration front of CO_2 back into the column [32]. In polar zeolites, the co-adsorption of N_2 is very weak, as a consequence repressurizing with N_2 hardly affects the CO_2 concentration front. It is therefore impossible to avoid the very low regeneration pressures in VSA cycles with highly selective adsorbents. Since recovery is intimately related to the regeneration pressure and since the power consumption of the VSA process increases with decreasing regeneration pressure, we can now understand why a higher recovery leads to higher operating costs.

3.2 VSA Simulations

From our experimental screening of zeolites, two materials emerged as the most attractive candidates for a CO_2 capture application: zeolite NaX has a very high CO_2 affinity and a high adsorption capacity but is difficult to regenerate; zeolite EMC-1 has a moderate adsorption capacity but exhibits excellent regenerability. Both have a high CO_2/N_2 selectivity. We have, therefore, decided to confront the behavior of EMC-1 and NaX in a VSA cycle by numerical simulations. The flue gas was represented by a mixture of 13.5% CO_2 in N_2 . For the sake of simplicity, a dry feed was used, *i.e.* it was

assumed that water has been removed from the flue gas upstream of the VSA. The single component adsorption isotherms of CO_2 and N_2 on NaX were taken from the literature [23], the isotherms of EMC-1 were in-house data. The experimental isotherms were modeled by a dual or single site Langmuir model:

$$q_j = \sum_i q_{sat,i} \cdot \frac{b_{j,i} \cdot p_j}{1 + b_{j,i} \cdot p_j}$$

$$b_{j,i} = b_{j,i,0} \cdot \exp\left(\frac{-h_{ads,j,i}}{RT}\right)$$

The parameters are given in Table 3.

TABLE 3

Parameters of the single or dual site Langmuir model used to fit the experimental isotherms of CO_2 and N_2

		q_{sat} (mol/kg)	b_0 (Pa^{-1})	h_{ads} (kJ/mol)
NaX	CO_2	2.09	3.84×10^{-10}	-40
		4.11	8.75×10^{-12}	-40
EMC-1	CO_2	6.25	3.81×10^{-10}	-19
		3.34	3.24×10^{-9}	-25
	N_2	4.15	4.70×10^{-10}	-25
	N_2	3.81	4.35×10^{-10}	-18

A simple extended Langmuir equation was used for modeling the co-adsorption of CO_2 and N_2 :

$$q_j = q_{sat,j,1} \cdot \frac{b_{j,1} \cdot p_j}{1 + \sum_m b_{m,1} \cdot p_m} + q_{sat,j,2} \cdot \frac{b_{j,2} \cdot p_j}{1 + \sum_m b_{m,2} \cdot p_m}$$

This is not the most precise co-adsorption model but is sufficiently accurate for a qualitative comparison of NaX and EMC-1. Since we were mainly interested in identifying the effect of the adsorption isotherms on the performance, we chose conditions under which mass transfer effects are totally negligible, *i.e.* a fairly long contact time of 0.4 s. The maximum gas velocity was fixed *via* the constraint of avoiding fluidization of the adsorbent particles and the column height was limited by the pressure drop (which should be below 0.2 bar). The adsorber column was considered to be adiabatic and the pressure drop in the column was neglected in the simulation. Further details of the model and its underlying assumptions are given in the Appendix. The VSA cycle was chosen based on the considerations above: an adsorption step, at $P_H = 1.2$ bar (to overcome the pressure drop in the column) and 323 K was followed by a co-current depressurization to P_R . The objective of the depressurization step was to remove N_2 from the interstitial volume of the column. The depressurization was followed by a rinse with part of the recovered CO_2 stream. In the next step, CO_2 was produced by lowering

the pressure to P_L , *i.e.* by pulling vacuum on the column. Part of the CO₂ that is recovered during this step is recycled to another column, for performing the CO₂ rinse. For this purpose, CO₂ must be compressed from P_L to P_R . Finally the column is repressurized, first with effluent of a column in depressurization and finally with the feed.

The most influential operating parameters of the VSA cycle were:

- the value of P_L : as explained above, it had a huge influence on recovery;
- the value of P_R : it had a large influence on the purity of CO₂;
- the duration of the adsorption and rinse steps.

These four parameters were varied in order to achieve our target values of 90% recovery and 96% purity. We found that, thanks to the high selectivity of NaX and EMC-1, a CO₂ rinse step was actually not necessary. The 96% purity of CO₂ could be achieved simply by optimizing the final pressure of the depressurization step.

Table 4 shows the conditions under which the target recovery and purity were achieved for NaX and EMC-1. The values of the key parameters t_{ads} , P_p and P_L , were surprisingly close for the two materials. As a consequence, productivity and power consumption for the evacuation step were also quite similar. The working capacities, *i.e.* the amounts of CO₂ adsorbed in each cycle, were 0.70 and 0.75 mol/kg for NaX and EMC-1, respectively. Remember that our screening experiments had yielded cyclic capacities of 1.8 and 1.2 mol/kg for NaX and EMC-1, respectively. Two factors may degrade the working capacity in the VSA simulations compared to the cyclic capacity obtained in our screening. First of all, temperature rise in adsorption and the temperature drop in desorption diminishes the capacity of the bed compared to isothermal operation. Secondly, the equilibrium capacity of the bed is not fully exploited because the mass transfer zone of CO₂ must be contained in the bed in order to achieve a high recovery of CO₂.

TABLE 4

Results of the simulations of a VSA cycle for CO₂ capture, using either NaX or EMC-1 as adsorbent

	NaX	EMC-1
$t_{ads}^{(a)}$ (s)	450	480
P_p (bar)	0.55	0.4
P_L (bar)	0.014	0.015
Purity CO ₂	96.7%	95.9%
Recovery CO ₂	89.9%	89.8%
Power consumption ^(b) (kJ/mol CO ₂)	11.7	11.0

^a Feed rate = 60 000 Nm³/h, column volume = 25.13 m³.

^b Power consumption during the CO₂ production step.

In order to evaluate the importance of these two effects, we have calculated the theoretical working capacity at equilibrium, first under isothermal and then under adiabatic conditions. For calculating the theoretical isothermal working capacity, we assumed that the whole adsorbent is in equilibrium with $P_H \times 0.135 = 0.16$ bar CO₂ and with $P_L = 0.014$ bar CO₂ at the end of the adsorption step and of the desorption step, respectively. The difference between these two equilibrium adsorbed amounts yielded the theoretical working capacity. The theoretical capacities were 1.7 and 1.3 mol/kg for NaX and EMC-1, respectively, *i.e.* close to the experimental cyclic capacities (Tab. 5). Co-adsorption of N₂ had a negligible impact on the theoretical working capacity. The good agreement between theoretical and experimental working capacities implies that our screening method was pertinent. As a next step, the adsorption isotherms were transposed into an adiabates [33], by accounting for the temperature rise caused by the exothermicity of adsorption, and the associated decrease of the adsorption capacity. For calculating the theoretical adiabatic working capacity, we assumed that the whole adsorbent is in equilibrium with $P_H \times 0.135 = 0.16$ bar CO₂ at 323 K + $\Delta T/2$ at the end of the adsorption step, and that the whole adsorbent is in equilibrium with $P_L = 0.014$ bar at 323 K – $\Delta T/2$. ΔT is the temperature swing between adsorption and desorption. The adiabatic capacities were 0.7 and 0.9 mol/kg for NaX and EMC-1, respectively. The working capacity of NaX dropped by 60% when the thermal effects were taken into account. The impact of adiabatic operation on the working capacity of EMC-1 was much smaller because its heat of adsorption is lower. The VSA simulations confirmed that the temperature swing between adsorption and desorption was indeed higher in the case of NaX (Fig. 8).

TABLE 5

Working capacities of NaX and EMC-1: experimental estimation by adsorption – desorption experiments, theoretical calculation under isothermal and adiabatic conditions and values obtained in the VSA simulations

Working capacity (mol/kg)	NaX	EMC-1
Experimental screening	1.8	1.2
Theoretical isothermal	1.75	1.35
Theoretical adiabatic	0.7	0.9
VSA simulations	0.7	0.75

The theoretical adiabatic working capacities were fairly close to the simulated working capacities, which means that they are a good qualitative indicator of the performance of an adsorbent. Still, the theoretical values predict that EMC-1 should perform slightly better than NaX in adiabatic operation, but in the VSA simulations both solids were equivalent. The explanation can be found in the concentration profiles (Fig. 9).

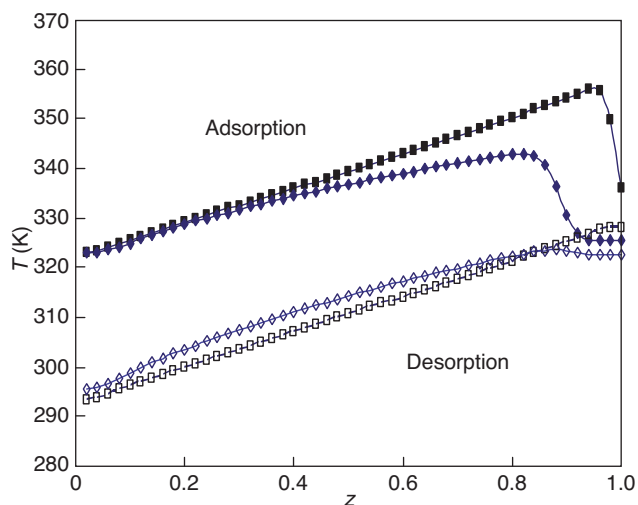


Figure 8

Temperature profile along the column axis z (adimensionalized) at the end of the adsorption step (full symbols) and at the end of the desorption step (empty symbols). NaX (squares) vs. EMC-1 (diamonds).

The mass transfer zone in the EMC-1 column was significantly larger than in the NaX column, *i.e.* the capacity of the bed was less well exploited. The CO_2/N_2 co-adsorption isotherm of EMC-1 is less favorable than that of NaX and this leads to a stronger dispersion of the CO_2 concentration front at low concentrations.

In summary, the moderate CO_2 affinity of EMC-1 compared to NaX was an advantage, because it diminished the temperature excursions in the column and therefore led to a higher theoretical working capacity under adiabatic conditions. In practice part of this advantage was lost, because the less favorable CO_2 isotherm of EMC-1 led to a broader mass transfer zone, hence the bed was less well exploited. Overall, the effects cancelled each other and the performance of both solid was quasi equivalent. In practice, one would probably stick with NaX as the preferred adsorbent since its preparation is easier and cheaper.

3.3 Industrial Feasibility

The major asset of VSA technology for CO_2 capture is the fact that the energy consumption of process is, at least theoretically, very low. According to our simulations under idealized conditions, *i.e.* under total absence of mass transfer limitations, the power consumption of the vacuum pump and the blower used for compressing the feed to 1.2 bar amounts to only 0.35 GJ/t CO_2 . This theoretical value is lower than recently published estimates (also based on simulation data) [27], because in our case a high recovery and purity of CO_2 could be achieved without using a CO_2 rinse step (the recycling

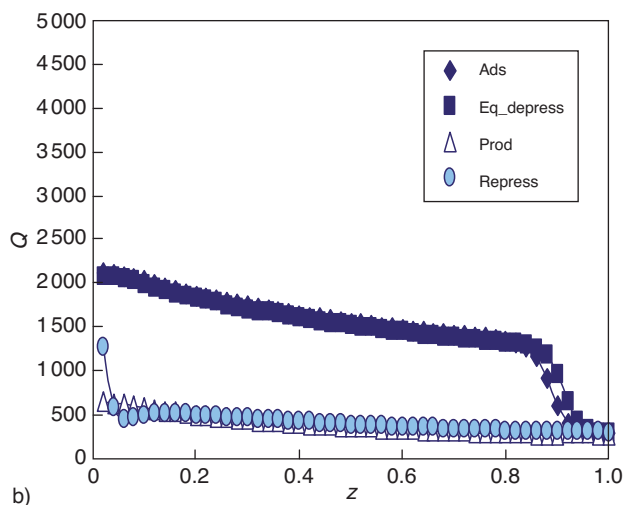
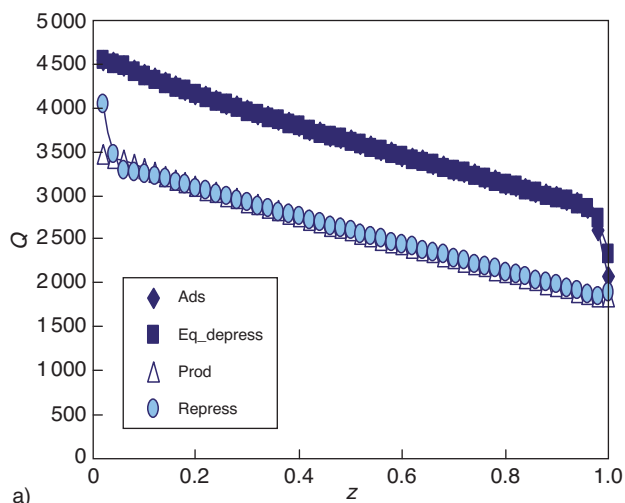


Figure 9

Axial concentration profiles of CO_2 in the adsorbed phase Q (in $\text{mol}/\text{m}^3\text{crystal}$) at the end of the different steps of the cycle: ads = adsorption, eq_depress = co-current depressurization, prod = production of CO_2 , repress = repressurization with feed. a) NaX (squares), b) EMC-1 (diamonds).

of CO_2 consumed additional energy). Yet, the simulated theoretical values are overly optimistic because they assume a 100% efficiency of the (vacuum) blowers. Experimentally measured energy consumptions are a factor of 4-5 higher than the theoretical values [34, 35]. Moreover, one has to be careful when comparing the electrical energy used by blowers with thermal energy used in temperature swing processes, as absorption by MEA. Electrical energy is produced from thermal energy with an efficiency of $\sim 40\%$, it is therefore more “expensive”. When both of these factors are taken into account, the energy balance of the VSA process is not that favorable any more.

In addition, application of the VSA technology on a large scale (*i.e.* the scale required for a 600 MW power plant) faces serious technological problems, which are rarely taken into account in the literature. The flue gas flow rate in a 600 MW power plant is in the order of 1.8×10^6 Nm³/h. In order to be able to treat this enormous flow rate, while keeping the pressure drop over the column low, huge cross sections are needed. If we extrapolate our simulations to the above-mentioned feed flow rate, the total cross section of the adsorbers should be 1500 m². The actual value should be lower because we carried out our simulations at fairly low gas velocities so as to avoid any mass transfer limitation. For comparison, Lively *et al.* [36] estimated the cross section of fixed bed adsorbers to be 850 m², if a pressure drop of 0.69 bar is authorized. These huge cross sections ask for new concepts in adsorber design, for example, structured adsorbent beds, where the adsorbents are packed into hollow fibers [34, 36, 37]. Such solutions are not yet industrial standard.

Another concern that must be raised about CO₂ capture by VSA is the very low pressure that must be used for desorption of CO₂ in order to assure a high recovery (see above). At 0.014 bar, the volume flow rate of the recovered CO₂ stream is 10 times higher than the volume flow rate of the feed. A large number of pumps must be installed in parallel in order to be able to cope with this huge volume flow and several compression stages are probably needed to raise the pressure of the recovered CO₂ stream back to 1 bar (pressure at which CO₂ is released in the reference MEA process). The high capital expenses associated with the installation of a large number of blowers, as well as the technological difficulty of dealing with the huge volume flow rates encountered during CO₂ recovery may render CO₂ capture by VSA processes economically unviable. A way to circumvent to low pressure desorption is to use dual-reflux systems [38-41]. In dual-reflux pressure swing separations, the feed is injected at an intermediate point of the column. Light product (N₂) is recycled to the top of the column and heavy product (CO₂) is recycled to the bottom of the column. In this way, both light and heavy product can be obtained at high recovery and purity, at desorption pressures as high as 0.3 bar [38, 41]. We are, however, not aware of any existing industrial unit that has been constructed according to a dual-reflux design.

CONCLUSIONS

One of the objectives of the present work was to tune the adsorption properties of zeolites so as to optimize their performance in post-combustion CO₂ capture. Our results show that it is possible to modulate the CO₂ adsorption isotherms of zeolites by changing the content of extra-framework Na⁺ cations and/or the zeolite structure (*i.e.* the pore size and pore geometry). Within a given zeolite structure, reducing the extra-framework cation content reduces the adsorption

capacity at low pressure but improves the regenerability. The CO₂/N₂ selectivity is not measurably affected as long as the Na⁺ content is above a certain threshold (which is around 2% wt Na for faujasite zeolites). Among the series of faujasite and mordenite zeolites that we have tested, the faujasites NaX (Si/Al = 1.3) and Na-EMC-1 (Si/Al = 3.9) present the best working capacity in cyclic adsorption – desorption experiments. Zeolite NaX has a very high CO₂ affinity, a high heat of adsorption and a high adsorption capacity but is difficult to regenerate; zeolite EMC-1 has a moderate adsorption capacity (and a moderate heat of adsorption) but exhibits excellent regenerability. Both solids exhibit a high CO₂/N₂ selectivity. Under isothermal conditions, the working capacity of zeolite NaX is about 50% higher than that of zeolite EMC-1. In adiabatic operation, the ranking is inversed. The higher heat of adsorption of CO₂ on NaX (compared to EMC-1) leads to higher temperature excursions in the bed during adsorption and desorption, and thereby strongly degrades the adsorption capacity of NaX [25, 26], even below the value of EMC-1. Simulations of a VSA cycle for CO₂ capture show, however, that the small theoretical advantage of EMC-1 is lost because the less favorable CO₂ isotherm of EMC-1 leads to a broader mass transfer zone, hence the bed is less well exploited.

From an application point of view, the main asset of VSA technology for CO₂ capture is the fact that the energy consumption of the process could, at least theoretically, be very low. There are, however, many technological hurdles to be overcome before VSA for CO₂ capture can become an industrial reality. Vacuum blowers are needed that can cope with huge volumetric flow rates and adsorber design has to be reinvented in order to minimize the pressure drop in the system. An additional obstacle is that the flue gas must be dried within or upstream of the VSA system, because all of the most promising CO₂ adsorbents largely prefer the adsorption of H₂O over the adsorption of CO₂. It is, therefore, highly uncertain whether CO₂ capture by VSA technology for large scale power plants can be economically and technically viable in the near future.

ACKNOWLEDGMENTS

Charles Leroux and Nicolas Bats are gratefully acknowledged for the synthesis of zeolite EMC-1.

REFERENCES

- 1 Raynal L., Bouillon P.A., Gomez A., Broutin P. (2011) From MEA to demixing solvents and future steps, a roadmap for lowering the cost of post-combustion carbon capture, *Chem. Eng. J.* **171**, 3, 742-752.
- 2 Knudsen J.N., Jensen P.J., Vilhelmsen P.J., Biede O. (2009) Experience with CO₂ capture from coal flue gas in pilot-scale: Testing of different amine solvents, *Energy Procedia* **1**, 783-790.

- 3 Serna-Guerrero R., Belmabkhout Y., Sayari A. (2010) Further investigations of CO₂ capture using triamine-grafted pore-expanded mesoporous silica, *Chem. Eng. J.* **158**, 3, 513-519.
- 4 Serna-Guerrero R., Belmabkhout Y., Sayari A. (2010) Triamine-grafted pore-expanded mesoporous silica for CO₂ capture: Effect of moisture and adsorbent regeneration strategies, *Adsorption* **16**, 6, 567-575.
- 5 Belmabkhout Y., Sayari A. (2010) Isothermal versus Non-isothermal Adsorption-Desorption Cycling of Triamine-Grafted Pore-Expanded MCM-41 Mesoporous Silica for CO₂ Capture from Flue Gas, *Energy Fuels* **24**, 5273-5280.
- 6 Drese J.H., Choi S., Lively R.P., Koros W.J., Fauth D.J., Gray M.L., Jones C.W. (2009) Synthesis-Structure-Property Relationships for Hyperbranched Aminosilica CO₂ Adsorbents, *Adv. Funct. Mater.* **19**, 23, 3821-3832.
- 7 Ebner A.D., Gray M.L., Chisholm N.G., Black Q.T., Mumford D.D., Nicholson M.A., Ritter J.A. (2011) Suitability of a Solid Amine Sorbent for CO₂ Capture by Pressure Swing Adsorption, *Ind. Eng. Chem. Res.* **50**, 9, 5634-5641.
- 8 Li B., Jiang B., Fauth D.J., Gray M.L., Pennline H.W., Richards G.A. (2011) Innovative nano-layered solid sorbents for CO₂ capture, *Chem. Commun.* **47**, 6, 1719-1721.
- 9 Gray M.L., Hoffman J.S., Hreha D.C., Fauth D.J., Hedges S.W., Champagne K.J., Pennline H.W. (2009) Parametric Study of Solid Amine Sorbents for the Capture of Carbon Dioxide, *Energy Fuels* **23**, 4840-4844.
- 10 Jones C.W., Maginn E.J. (2010) Materials and Processes for Carbon Capture and Sequestration, *Chemsuschem.* **3**, 8, 863-864.
- 11 Hiyoshi N., Yogo K., Yashima T. (2005) Adsorption characteristics of carbon dioxide on organically functionalized SBA-15, *Micropor. Mesopor. Mater.* **84**, 1-3, 357-365.
- 12 Gray M.L., Champagne K.J., Fauth D., Baltrus J.P., Pennline H. (2008) Performance of immobilized tertiary amine solid sorbents for the capture of carbon dioxide, *Int. J. Greenhouse Gas Control* **2**, 1, 3-8.
- 13 Sircar S., Golden T.C. (1995) Isothermal and Isobaric Desorption of Carbon-Dioxide by Purge, *Ind. Eng. Chem. Res.* **34**, 8, 2881-2888.
- 14 Kim J.-N., Chue K.-T., Kim K.I., Cho S.-H., Kim J.-D. (1994) Non-isothermal Adsorption of Nitrogen-Carbon Dioxide Mixture in a Fixed Bed of Zeolite-X, *J. Chem. Eng. Japan* **27**, 45-51.
- 15 Merel J., Clausse M., Meunier F. (2008) Experimental investigation on CO₂ post-combustion capture by indirect thermal swing adsorption using 13X and 5A zeolites, *Ind. Eng. Chem. Res.* **47**, 1, 209-215.
- 16 Liu J., Wang Y., Benin A.I., Jakubczak P., Willis R.R., Levan M.D. (2010) CO₂/H₂O Adsorption Equilibrium and Rates on Metal-Organic Frameworks: HKUST-1 and Ni/DOBDC, *Langmuir* **26**, 17, 14301-14307.
- 17 Li G., Xiao P., Webley P., Zhang J., Singh R., Marshall M. (2008) Capture of CO₂ from high humidity flue gas by vacuum swing adsorption with zeolite 13X, *Adsorption* **14**, 2-3, 415-422.
- 18 Trzpit M., Soulard M., Patarin J., Desbiens N., Cailliez F., Boutin A., Demachy I., Fuchs A.H. (2007) The effect of local defects on water adsorption in silicalite-1 zeolite: A joint experimental and molecular simulation study, *Langmuir* **23**, 20, 10131-10139.
- 19 Dunne J.A., Mariwala R., Rao M., Sircar S., Gorte R.J., Myers A.L. (1996) Calorimetric heats of adsorption and adsorption isotherms .1. O₂, N₂, Ar, CO₂, CH₄, C₂H₆ and SF₆ on silicalite, *Langmuir* **12**, 24, 5888-5895.
- 20 Palomino M., Corma A., Rey F., Valencia S. (2010) New Insights on CO₂ – Methane Separation Using LTA Zeolites with Different Si/Al Ratios and a First Comparison with MOFs, *Langmuir* **26**, 3, 1910-1917.
- 21 Chatelain T., Patarin J., Soulard M., Guth J.L., Schultz P. (1995) Synthesis and characterization of high-silica EMT and FAU zeolites prepared in the presence of crown-ethers with either ethylene-glycol or 1,3,5-trioxane, *Zeolites* **15**, 90
- 22 Belmabkhout Y., Pirngruber G., Jolimaitre E., Methivier A. (2007) A complete experimental approach for synthesis gas separation studies using static gravimetric and column breakthrough experiments, *Adsorption* **13**, 3-4, 341-349.
- 23 Dunne J.A., Rao M., Sircar S., Gorte R.J., Myers A.L. (1996) Calorimetric heats of adsorption and adsorption isotherms. 2. O₂, N₂, Ar, CO₂, CH₄, C₂H₆, and SF₆ on NaX, H-ZSM-5, and Na-ZSM-5 zeolites, *Langmuir* **12**, 24, 5896-5904.
- 24 Li G., Xiao P., Webley P.A., Zhang J., Singh R. (2009) Competition of CO₂/H₂O in adsorption based CO₂ capture, *Energy Procedia* **1**, 1, 1123-1130.
- 25 Zhang J., Webley P.A. (2008) Cycle development and design for CO₂ capture from flue gas by vacuum swing adsorption, *Environ. Sci. Technol.* **42**, 2, 563-569.
- 26 Zhang J., Webley P.A., Xiao P. (2008) Effect of process parameters on power requirements of vacuum swing adsorption technology for CO₂ capture from flue gas, *Energy Convers. Manage.* **49**, 2, 346-356.
- 27 Liu Z., Grande C.A., Li P., Yu J.G., Rodrigues A.E. (2011) Multi-bed vacuum pressure swing adsorption for carbon dioxide capture from flue gas, *Sep. Purif. Technol.* **81**, 3, 307-317.
- 28 Park J.H., Beum H.T., Kim J.N., Cho S.H. (2002) Numerical analysis on the power consumption of the PSA process for recovering CO₂ from flue gas, *Ind. Eng. Chem. Res.* **41**, 16, 4122-4131.
- 29 Chue K.T., Kim J.N., Yoo Y.J., Cho S.H., Yang R.T. (1995) Comparison of Activated Carbon and Zeolite 13X for CO₂ Recovery from Flue-Gas by Pressure Swing Adsorption, *Ind. Eng. Chem. Res.* **34**, 2, 591-598.
- 30 Na B.K., Lee H., Koo K.K., Song H.K. (2002) Effect of rinse and recycle methods on the pressure swing adsorption process to recover CO₂ from power plant flue gas using activated carbon, *Ind. Eng. Chem. Res.* **41**, 22, 5498-5503.
- 31 Dantas T.L.P., Luna F.M.T., Silva I.J., Torres A.E.B., de Azevedo D.C.S., Rodrigues A.E., Moreira R.F.P.M. (2011) Carbon dioxide-nitrogen separation through pressure swing adsorption, *Chem. Eng. J.* **172**, 2-3, 698-704.
- 32 Kikkinides E.S., Yang R.T., Cho S.H. (1993) Concentration and recovery of CO₂ from flue-gas by pressure swing adsorption, *Ind. Eng. Chem. Res.* **32**, 11, 2714-2720.
- 33 Pirngruber G.D., Hamon L., Bourrelly S., Llewellyn P.L., Lenoir E., Guillerm V., Serre C., Devic T. (2012) A Method for Screening the Potential of MOFs as CO₂ Adsorbents in Pressure Swing Adsorption Processes, *Chemsuschem.* **5**, 4, 762-776.
- 34 Liu Z., Wang L., Kong X., Li P., Yu J., Rodrigues A.E. (2012) Onsite CO₂ Capture from Flue Gas by an Adsorption Process in a Coal-Fired Power Plant, *Ind. Eng. Chem. Res.* **51**, 21, 7355-7363.
- 35 Cho S.-H., Park J.H., Beum H.T., Han S.-S., Kim J.-N. (2004) A 2-stage PSA Process for the Recovery of CO₂ from Flue Gas and its Power Consumption, *Stud. Surf. Sci. Catal.* **153**, 405-410.
- 36 Lively R.P., Chance R.R., Koros W.J. (2010) Enabling Low-Cost CO₂ Capture via Heat Integration, *Ind. Eng. Chem. Res.* **49**, 16, 7550-7562.
- 37 Lively R.P., Chance R.R., Kelley B.T., Deckman H.W., Drese J.H., Jones C.W., Koros W.J. (2009) Hollow Fiber Adsorbents for CO₂ Removal from Flue Gas, *Ind. Eng. Chem. Res.* **48**, 15, 7314-7324.
- 38 Sivakumar S.V., Rao D.P. (2011) Modified Duplex PSA. 1. Sharp Separation and Process Intensification for CO₂-N₂-13X Zeolite System, *Ind. Eng. Chem. Res.* **50**, 6, 3426-3436.

- 39 Kearns D.T., Webley P.A. (2006) Modelling and evaluation of dual-reflux pressure swing adsorption cycles: Part I. Mathematical models, *Chem. Eng. Sci.* **61**, 22, 7223-7233.
- 40 Diagne D., Goto M., Hirose T. (1994) New PSA Process with Intermediate Feed Inlet Position Operated with Dual Refluxes – Application to Carbon-Dioxide Removal and Enrichment, *J. Chem. Eng. Japan* **27**, 1, 85-89.
- 41 Diagne D., Goto M., Hirose T. (1995) Parametric Studies on CO₂ Separation and Recovery by a Dual Reflux PSA Process Consisting of Both Rectifying and Stripping Sections, *Ind. Eng. Chem. Res.* **34**, 9, 3083-3089.
- 42 Leinekugel-le-Cocq D., Tayakout-Fayolle M., Le Gorrec Y., Jallut C. (2007) A double linear driving force approximation for non-isothermal mass transfer modeling through bi-disperse adsorbents, *Chem. Eng. Sci.* **62**, 15, 4040-4053.
- 43 Farooq S., Ruthven D.M., Boniface H.A. (1989) Numerical simulation of a pressure swing adsorption oxygen unit, *Chem. Eng. Sci.* **44**, 12, 2809-2816.

*Final manuscript received in October 2012
Published online in August 2013*

Copyright © 2013 IFP Energies nouvelles

Permission to make digital or hard copies of part or all of this work for personal or classroom use is granted without fee provided that copies are not made or distributed for profit or commercial advantage and that copies bear this notice and the full citation on the first page. Copyrights for components of this work owned by others than IFP Energies nouvelles must be honored. Abstracting with credit is permitted. To copy otherwise, to republish, to post on servers, or to redistribute to lists, requires prior specific permission and/or a fee: Request permission from Information Mission, IFP Energies nouvelles, fax. +33 1 47 52 70 96, or revueogst@ifpen.fr.

APPENDIX

The cyclic PSA model is based on the non-isothermal adsorption column model described by Leinekugel-le-Cocq *et al.* [42]. It is summarized in Table A1 and Table A2. The main assumptions of the bed model are:

- the ideal gas law is obeyed;
- the pressure drop in the bed is negligible;
- the flow in the packed bed is represented by a cascade of CSTR (Continuous Stirred Tank Reactors) in series; 101 reactors have been used in the following simulations corresponding to a Péclet number of approximately 200;
- the adsorbent pellets have a bi-modal pore size distribution (micro- and macropores), and the intra-particle mass transfer is described by the modified double linear driving force model;
- chemical kinetic time constant is small compare to mass transfer time constant in the particle;
- adsorption equilibrium are modeled considering extended multi-component Langmuir isotherms.

During pressurization and blow-down steps, we consider that the total pressure in the bed changes linearly with time [43]:

$$P(t) = P_I^{step} + (P_F^{step} - P_I^{step}) \frac{t - t_I^{step}}{\Delta t_{step}} \quad (1)$$

The computing code based on this model has been developed in Fortran. The ordinary differential equations system obtained by spatial discretization by a cascade of CSTRs is solved using the DDASPK subroutine based on the Petzold-Gear BDF method.

TABLE A1
Cyclic PSA model

Models	Equations
CO ₂ bulk phase mass balance	$\frac{\partial c_{CO_2}}{\partial t} = -\frac{1}{\varepsilon} \cdot \frac{\partial(u \cdot c_{CO_2})}{\partial z} - \frac{1-\varepsilon}{\varepsilon} \cdot \varepsilon_p \cdot a_s^p \cdot N_{CO_2}^{mac}$
Bulk phase energy balance	$\frac{\partial T_g}{\partial t} = -\frac{u}{\varepsilon} \cdot \frac{\partial T_g}{\partial z} + \frac{1}{C_{P,g}} \cdot \frac{\partial P}{\partial t} - \frac{1-\varepsilon}{\varepsilon} \cdot \frac{a_s^p \cdot k_{th}}{C_{P,g}} \cdot (T_g - T_s) - \frac{1}{C_{P,g}} \cdot \frac{2 \cdot k_w}{\varepsilon \cdot R_{int}} \cdot (T_g - T_w)$ with $C_{P,g} = \sum_{i=1}^{n_c} c_i \cdot C_{P,i}$
Superficial u velocity expression: overall mass balance	$\frac{1}{\varepsilon} \frac{\partial u}{\partial z} = -\frac{1-\varepsilon}{\varepsilon} \cdot \frac{a_s^p \cdot k_{th}}{C_{P,g}} \cdot \left(1 - \frac{T_s}{T_g}\right) - \frac{1}{C_{P,g}} \cdot \frac{2 \cdot k_w}{\varepsilon \cdot R_{int}} \cdot \left(1 - \frac{T_w}{T_g}\right)$ $+ \frac{\partial P}{\partial t} \cdot \left(\frac{1}{T_g} \frac{1}{C_{P,g}} - \frac{1}{P}\right) - \frac{1-\varepsilon}{\varepsilon} \cdot \varepsilon_p \cdot \left(\frac{R \cdot T_g}{P}\right) \cdot a_s^p \cdot N_T^{mac}$
CO ₂ macroporous phase mass balance	$\frac{\partial c^{mac}}{\partial t} = a_s^p \cdot N_{CO_2}^{mac} - \frac{1-\varepsilon_p}{\varepsilon_p} \cdot a_s^c \cdot N_{CO_2}^{ads}$
N_T^{mac} expression: overall mass balance in macroporous phase	$N_T^{mac} = \frac{1}{a_s^c} \left(-\frac{P}{R \cdot T_s^2} \cdot \frac{\partial T_s}{\partial t} + \frac{1}{R \cdot T_s} \cdot \frac{\partial P}{\partial t} + \frac{1-\varepsilon_p}{\varepsilon_p} \cdot a_s^c \cdot N_{CO_2}^{ads} \right)$
CO ₂ adsorbed phase mass balance	$\underbrace{\left(\frac{\partial q}{\partial c^*} \right)_{T_s} \cdot \frac{\partial c^*}{\partial t} + \left(\frac{\partial q}{\partial T_s} \right)_{c^*} \cdot \frac{\partial T_s}{\partial t}}_{\frac{\partial q}{\partial t}} = a_s^c \cdot N_{CO_2}^{ads}$
Particle energy balance	$\frac{\partial T_s}{\partial t} = \frac{a_s^c}{(1-\varepsilon_p) \cdot \rho_s \cdot C_s} \cdot N_{CO_2}^{ads} \cdot (-\Delta H_{CO_2}^{ads}) + \frac{a_s^p \cdot k_{th}}{(1-\varepsilon_p) \cdot \rho_s \cdot C_s} \cdot (T_g - T_s)$

TABLE A2

Intra-granular mass transfer molar flux and equilibrium

Models	Equations
CO ₂ molar flow rate between bulk and macroporous phases	$N_{\text{CO}_2}^{\text{mac}} = N_T^{\text{mac}} \cdot \frac{x_{\text{CO}_2}^{\text{mac}} \cdot e^{-N_T^{\text{mac}} \left(\frac{\delta_f}{D_{\text{CO}_2}^f \cdot c_T} + \frac{\delta_{\text{mac}}}{D_{\text{CO}_2}^{\text{mac}} \cdot c_T^{\text{mac}}} \right)} - x_{\text{CO}_2}}{e^{-N_T^{\text{mac}} \left(\frac{\delta_f}{D_{\text{CO}_2}^f \cdot c_T} + \frac{\delta_{\text{mac}}}{D_{\text{CO}_2}^{\text{mac}} \cdot c_T^{\text{mac}}} \right)} - 1}$
CO ₂ molar flow rate between macroporous and adsorbed phases	$N_{\text{CO}_2}^{\text{ads}} = \frac{5}{R_c} \cdot D_{\text{CO}_2}^c \cdot \left(\frac{\partial q}{\partial c^*} \right)_{T_g} \cdot (c^{\text{mac}} - c^*)$
Adsorption isotherm	$\frac{q_{\text{CO}_2}}{q_{\text{sat}}} = \frac{b \cdot c^*}{1 + b \cdot c^*} \quad \text{with} \quad b = b_0 \cdot T_s \cdot e^{\frac{\Delta H_{\text{CO}_2}^{\text{ads}}}{RT_s}}$